THE JOURNAL OF BIOLOGICAL CHEMISTRY VOL. 287, NO. 18, pp. 14937–14949, April 27, 2012

Intramolecular Fluorescence Resonance Energy Transfer (FRET) Sensors of the Orexin OX_1 and OX_2 Receptors Identify Slow Kinetics of Agonist Activation*[S]

Received for publication, December 15, 2011, and in revised form, February 14, 2012 Published, JBC Papers in Press, March 2, 2012, DOI 10.1074/jbc.M111.334300

Tian-Rui Xu, Richard J. Ward, John D. Pediani, and Graeme Milligan[1]

From the Molecular Pharmacology Group, Institute of Molecular, Cell and Systems Biology, College of Medical, Veterinary and Life Sciences, University of Glasgow, Glasgow G12 8QQ, Scotland, United Kingdom

Background: Orexin receptors are potential targets for the treatment of narcolepsy and insomnia.
Results: Intramolecular FRET sensor forms of these receptors were functional and able to report the kinetics of agonist-mediated activation.
Conclusion: The 33 amino acid peptide orexin A activates the receptors slowly.
Significance: Such sensors provide a unique means to explore the kinetics of receptor activation.

Intramolecular fluorescence resonance energy transfer (FRET) sensors able to detect changes in distance or orientation between the 3rd intracellular loop and C-terminal tail of the human orexin OX_1 and OX_2 G protein-coupled receptors following binding of agonist ligands were produced and expressed stably. These were directed to the plasma membrane and, despite the substantial sequence alterations introduced, in each case were able to elevate $[Ca^{2+}]_i$, promote phosphorylation of the ERK1/2 MAP kinases and become internalized effectively upon addition of the native orexin peptides. Detailed characterization of the OX_1 sensor demonstrated that it was activated with rank order of potency orexin A > orexin B > orexin A 16–33, that it bound antagonist ligands with affinity similar to the wild-type receptor, and that mutation of a single residue, D203A, greatly reduced the binding and function of orexin A but not antagonist ligands. Addition of orexin A to individual cells expressing an OX_1 sensor resulted in a time- and concentration-dependent reduction in FRET signal consistent with mass-action and potency/affinity estimates for the peptide. Compared with the response kinetics of a muscarinic M_3 acetylcholine receptor sensor upon addition of agonist, response of the OX_1 and OX_2 sensors to orexin A was slow, consistent with a multistep binding and activation process. Such sensors provide means to assess the kinetics of receptor activation and how this may be altered by mutation and sequence variation of the receptors.

The orexin peptides orexin A and orexin B are produced by neurons of the lateral hypothalamus from a common precursor and function via binding to and activating two members of the G protein-coupled receptor (GPCR)[2] superfamily, the OX_1 and OX_2 receptors (1–2), which share 64% sequence identity. These receptors have attracted considerable interest (3–6) not least because intracerebroventricular administration of orexin A to animals is known to stimulate food consumption and to increase wakefulness. Furthermore, because a genetic deficiency of the OX_2 receptor is associated with narcolepsy in dogs (7), and in some cases of this condition in man (8), it has been hypothesized that blockade of either this receptor alone or of a combination of the OX_1 and OX_2 receptors might provide a means to regulate sleep and to treat insomnia (1, 5, 9–11). A number of either OX_2 receptor-selective or combined OX_1/OX_2 receptor blockers have been developed, therefore, to assess this potential (9–12). Human orexin A is a 33 amino acid peptide, modified at both N and C termini, and with molecular mass 3562 Da, whereas orexin B is a 28 amino acid peptide of mass 2899 Da. As with a number of other GPCRs that respond to peptides of substantial size, it has clearly been difficult to identify small molecule agonist ligands for these receptors, because no such molecules have yet been described. This is despite analgesic effects of orexin A that suggest that orexin receptor agonists might be effective as anti-nociceptive therapeutics (4).

The synthesis of radiolabeled forms of a small number of OX_1 and OX_2 antagonists (13–14) has recently allowed preliminary analysis of the binding pocket for orexin A in the two receptors by comparing loss of agonist function of this peptide in mutants of the receptors that continue to bind the antagonist ligands with robust affinity (14). Despite this, rather little is known about either the mode or kinetics of binding of the orexin peptides, not least because competition binding studies between the synthetic radiolabeled antagonists and the peptide ligands have been difficult to establish (13).

Fluorescence resonance energy transfer (FRET) has been used widely to explore interactions between different proteins, including pairs of GPCRs, co-expressed in the same cell (15–17). Furthermore FRET between appropriately labeled ligands

* These studies were supported by the Medical Research Council UK (Grant G0900050).
[S] This article contains supplemental Figs. S1–S5.
[1] To whom correspondence should be addressed: 253 Wolfson Link Building, University of Glasgow, University Avenue, Glasgow G12 8QQ, Scotland, UK. Tel.: 44-141-330-5557; Fax: 44-141-330-5481; E-mail: Graeme.Milligan@glagow.ac.uk.

[2] The abbreviations used are: GPCR, G-protein-coupled receptor; CFP, cyan fluorescent protein; FlAsH, fluoroscein arsenical hairpin binder; FRET, fluorescence resonance energy transfer.

and forms of GPCRs with autofluorescent proteins inserted into the extracellular N-terminal domain has provided a means to explore aspects of the kinetics of ligand binding and the identification of novel receptor ligands (18–19). An alternative FRET approach that can detect activation of a GPCR in response to agonist ligands involves the construction of intramolecular FRET sensors. To date only a few examples have been reported (17, 20–23). These have been designed to report activation of the receptor upon agonist binding with the energy donor and acceptor species being introduced into areas on the intracellular face of the receptor that are believed to move relative to one another or re-orientate as part of the process of activation. Early versions of such sensors generally placed cyan fluorescent protein (CFP) inframe with the C-terminal tail of the receptor and engineered a yellow fluorescent protein (YFP) into a location within the third intracellular loop (20–21). More recently, the substantial bulk of YFP has been replaced by introduction of a fluoroscein arsenical hairpin binder (FlAsH) sequence, to which binding of an inherently non-fluorescent ligand generates a fluorescent species able to function as an energy acceptor from CFP (17, 22–23). Such intramolecular FRET sensors have detected rapid binding and de-binding of small molecules, such as mimetics of acetylcholine to muscarinic acetylcholine receptor subtypes (22–23) and to variants of these in which the ligand binding selectivity had been re-engineered by mutagenesis (23).

To date, the only receptors for peptide hormones for which intramolecular FRET sensors have been reported are the B2 bradykinin receptor (20) and the parathyroid hormone receptor (21). In the case of the B2 bradykinin receptor sensor, the potency of the native peptide agonist at the sensor was far removed from that of the unmodified receptor (20), raising questions as to the utility of the construct and the effects of the alterations made to the receptor to generate the sensor. For the parathyroid hormone receptor sensor there was less of an effect on peptide potency/affinity but, interestingly, it was noted that despite known high affinity, the peptide generated a FRET response much more slowly (21) than observed for small molecule agonists at catecholamine receptor sensors where the ligands are known to have modest affinity (22–23).

If peptide receptive GPCR sensors could be defined and engineered such that they retained function and pharmacology equivalent to the wild type receptor, they would be valuable tools to examine each of ligand binding kinetics, the details of receptor activation mechanisms, the effects of polymorphic variation in receptor sequence and of designed mutations. Furthermore, they might provide tools to explore the activation of receptors in both *ex vivo* and, eventually, *in vivo* settings. To explore such potential, herein, we report the production and detailed characterization of intramolecular FRET sensor forms of both the human orexin OX_1 and OX_2 receptors.

EXPERIMENTAL PROCEDURES

Drugs, Chemicals, Reagents, and Other Materials—Lipofectamine transfection reagent was from Invitrogen (Paisley, UK). [^{3}H]SB674042 ((1-(5-(2-fluoro-phenyl)-2-methyl-thiazol-4-yl)-1-((*S*)-2-(5-phenyl-(1,3,4)oxadiazol-2-ylmethyl)-pyrrolidin-1-yl)-methanone) was from Perkin Elmer (Boston, MA). SB334867 ((*N*-(2-methyl-6-benzoxazolyl)-*N*′-1,5-naphthyridin-4-yl urea), SB408124 (*N*-(6,8-difluoro-2-methyl-4-quinolinyl)-*N*′-[4-(dimethylamino)phenyl]urea) and TCS-OX2-29 *S*)-1-(3,4-dihydro-6,7-dimethoxy-2(1*H*)-isoquinolinyl)-3,3-dimethyl-2-[(4-pyridinylmethyl)amino]-1-butanone) were from Tocris Biosciences (Avonmouth, UK). Orexin A and orexin B were from Bachem (UK) Ltd (St Helens, Merseyside UK). Orexin A 16–33 was from Phoenix Pharmaceuticals INC (Burlingame, CA) or from Chinapeptides (Shanghai, China). Oligonucleotides were from ThermoElectron (Ulm, Germany). Flp-In™ T-REx™ 293 cells, Lipofectamine 2000 transfection reagent, TC-FlAsH II In-Cell Tetracysteine Tag Detection Kit and all materials for tissue culture were from Invitrogen. Anti-VSV-G and anti-HA were from Sigma. Protease inhibitor mixture tablets were from Roche Diagnostics (Mannheim, Germany). All other reagents were obtained from Fisher Scientific (Loughborough, UK) or Sigma Aldrich Co Ltd.

DNA Constructs—The VSV-G-SNAP-OX_1 construct has been described previously (24–25). Intramolecular FRET sensor forms of the human OX_1 and OX_2 receptors included a C-terminal CFP to act as energy donor, although in a number of examples, the C-terminal tail of the receptor was truncated to produce constructs with higher basal FRET signals. The FlAsH binding sequence FLNCCPGCCMEP, which once labeled acted as energy acceptor, was introduced at various locations in the 3rd intracellular loop of each receptor. In some cases this replaced an equivalent sequence of 12 amino acids and in others reduced the overall length of the loop; see "Results" and supplemental Fig. S1 for details. Constructs were ligated into either pcDNA3.1 for initial transient transfection studies, or into pcDNA5/FRT/TO (Invitrogen) to generate Flp-In™ T-REx™ 293 inducible stable cell lines (26).

Generation and Maintenance of Stable Flp-In™ T-REx™ 293 Cells—To generate Flp-In™ T-REx™ 293 cells able to inducibly express the FRET sensor constructs, cells were co-transfected with the plasmid pOG44 and the desired protein cDNA in pcDNA5/FRT/TO (Invitrogen) at a ratio of 9:1 using Lipofectamine (26). After 48 h, the medium was supplemented with 200 μg·ml^{-1} hygromycin to select for stably transfected cells. Pools of cells were established and tested for inducible expression by the addition of 1 μg·ml^{-1} doxycycline for 48 h followed by screening for fluorescence corresponding to CFP and for VSV-G protein expression by Western blotting.

HEK293T Cell Culture and Transfection—HEK293T cells were maintained in Dulbecco's modification of Eagle's medium (DMEM) supplemented with 0.292 g·liter^{-1} L-glutamine, 1% antibiotic mixture and 10% (v/v) newborn calf serum at 37 °C in a 5% CO_2 humidified atmosphere. The cells were transfected with various $OX_{1/2}$ FRET sensor constructs using Lipofectamine 2000 reagent according to protocols from the supplier. 48 h after transfection, cells were labeled with TC-FlAsH II In-Cell Tetracysteine Tag Detection Kit.

Cell Lysates and Western Blotting—Cells were washed once in cold PBS (120 mM NaCl, 25 mM KCl, 10 mM Na_2HPO_4, and 3 mM KH_2PO_4, pH7.4) and harvested with ice-cold RIPA buffer (radioimmunoprecipitation assay buffer, 50 mM HEPES, 150 mM NaCl, 1% Triton X-100, and 0.5% sodium deoxycholate, 10 mM NaF, 5 mM EDTA, 10 mM NaH_2PO_4, 5% ethylene glycol, pH

7.4) supplemented with Complete protease inhibitors mixture (Roche Diagnostics, Mannheim, Germany). Extracts were passed though a 25-gauge needle and incubated for 15 min at 4 °C while spinning on a rotating wheel. Cellular extracts were then centrifuged for 30 min at 14,000 × *g* and the supernatant was recovered. After heating samples at 65 °C for 5 min, both cell lysates and pulldowns were subjected to SDS-PAGE analysis using 4 to 12% Bis-Tris gels (NuPAGE; Invitrogen) and MOPS buffer. After separation, the proteins were electrophoretically transferred to nitrocellulose membrane, which was then blocked (5% fat-free milk powder in PBS with 0.1% Tween-20) at 4 °C on a rotating shaker overnight. The membrane was incubated for 3 h with primary antibody in 2% fat-free milk powder in PBS-Tween, washed (3 × 10 min PBS-Tween) and then incubated for 3 h with appropriate secondary antibody (horseradish peroxidase-linked donkey anti-rabbit IgG, sheep anti-mouse HRP or goat anti-rat HRP, GE Healthcare) diluted 1:10000 in 2% fat-free milk powder in PBS-Tween. After washing, proteins were detected by enhanced chemiluminescence (Pierce Protein Research Products, Thermo Scientific) according to the manufacturer's instructions.

Cell Membrane Preparation—Pellets of cells were frozen at −80 °C for a minimum of 1 h, thawed, and resuspended in ice-cold 10 mM Tris, 0.1 mM EDTA, pH 7.4 (TE buffer) supplemented with Complete protease inhibitors mixture (Roche Diagnostics). Cells were homogenized on ice by 40 strokes of a glass on Teflon homogenizer followed by centrifugation at 1000 × *g* for 5 min at 4 °C to remove unbroken cells and nuclei. The supernatant fraction was removed and passed through a 25-gauge needle 10 times before being transferred to ultracentrifuge tubes and subjected to centrifugation at 50,000 × *g* for 30 min at 4 °C. The resulting pellets were resuspended in ice-cold TE buffer. Protein concentration was assessed and membranes were stored at −80 °C until required.

[^{3}H]SB674042 Binding Assays (Membranes)—Saturation binding curves were established by the addition of 5 μg of membrane protein to assay buffer (25 mM HEPES, 0.5 mM EDTA, and 2.5 mM $MgCl_2$, pH 7.4, supplemented with 0.3% BSA) containing varying concentrations of [^{3}H]SB674042 (13, 23–24)(0.4–20 nM). Nonspecific binding was determined in the presence of 3 μM SB408124 or SB334867 as appropriate. Reactions were incubated for 90 min at 25°C, and bound ligand was separated from free by vacuum filtration through GF/C filters (Brandel Inc, Gaithersburg, MD). The filters were washed twice with cold 1xPBS (120 mM NaCl, 25 mM KCl, 10 mM Na_2HPO_4, 3 mM KH_2PO_4, pH 7.4) and bound ligand was estimated by liquid scintillation spectrometry. In competition binding studies varying concentrations of unlabeled ligands were co-added along with a single concentration of [^{3}H]SB674042.

[^{3}H]SB674042 Binding Assays (Intact Cells)—Cells were grown overnight, with doxycycline induction as required, on white 96-well plates, which had been treated with 0.1 mg·ml^{-1} poly-D-lysine. The medium was removed and replaced with 200 μl per well buffer containing 150 mM NaCl, 20 mM HEPES and 0.5% BSA, pH 7.4 with varying concentrations of [^{3}H]SB674042, (0.4–20 nM). Nonspecific binding was determined in the presence of 3 μM SB408124. The plates were incubated at 25 °C for 60 min and terminated by removal of the binding mixture, followed by washing with 3 × 200 μl per well, ice-cold 1× PBS. 100 μl per well Microscint 20 was added, and the plates sealed before incubation for 2 h at room temperature on a rapidly shaking platform. Bound ligand was determined using a Packard Topcount NXT. A number of equivalent wells were also included in the experiment. The medium was removed from these wells and the cells were trypsinized and counted using a Countess automated cell counter (Invitrogen, Paisley, UK). Using the specific binding per well and the number of cells per well, mol· [^{3}H]SB674042·cell^{-1} was determined.

Calcium Mobilization Assays—Flp-In™ T-REx™ 293 cells able to express the FRET constructs in an inducible manner were grown in poly-D-lysine coated, black, clear bottom 96-well microtiter plates. 24 h after induction with doxycycline, the cells were loaded with the calcium-sensitive dye Fura-2, by changing the media for DMEM containing 3 μM Fura-2. The plates were incubated in the dark for 45 min at 37 °C and then washed with 2 × 100 μl/well of HEPES buffer (130 mM NaCl, 5 mM KCl, 1 mM $CaCl_2$, 1 mM $MgCl_2$, 20 mM HEPES, and 10 mM D-glucose, pH7.4). 100 μl/well HEPES buffer was then added and the plate incubated at room temperature for 30 min in the dark. The effect of ligands was then assessed by measuring calcium response using a FLEX-Station (Molecular Devices, Sunnydale, CA) (24).

ERK1/2 MAP Kinase Phosphorylation—ERK1/2 MAP kinase phosphorylation assays were conducted in two independent ways. First, cells stably expressing sensors of interest were grown in 12-well plates, and rendered quiescent by serum starvation for 12 h prior to stimulation. Cells were then placed on ice and solubilized directly in 200 μl of Laemmli sample buffer. The samples were sonicated for 30 s, heated for 15 min at 95 °C, and microcentrifuged for 5 min before fractionation of the proteins on SDS/PAGE. Phosphorylation of ERK1/2 MAP kinases was detected by protein immunoblotting using a phospho-ERK1/2-specific antibody (Cell Signaling Technology, Nottingham, UK). The nitrocellulose membranes were subsequently stripped of immunoglobulins and re-probed using an anti-ERK1/2 antibody (Cell Signaling Technology) to assess the equivalence of protein loading.

Alternatively, Flp-In™ T-REx™ 293 cells able to express the FRET sensors were plated at a density of 40,000 cells per well in a poly-D-lysine coated 96-well plate. Expression of the construct under study was induced by the addition of 100 ng·ml^{-1} doxycycline. The cells were allowed to grow overnight and were then serum starved for 4 h prior to ligand stimulation as required. Cells were then treated with lysis buffer (SureFire AlphaScreen kit, Perkin Elmer (Boston, MA)) (25) and then processed according to the manufacturer's instructions.

Detection of Internalization (Fluorescent Microscopy)—Cells stably expressing an OX_1 sensor were grown on coverslips and placed in a microscope chamber containing physiological HEPES-buffered saline solution (130 mM NaCl, 5 mM KCl, 1 mM $CaCl_2$, 1 mM $MgCl_2$, 20 mM HEPES, and 10 mM D-glucose, pH 7.4) and treated with 10^{-7} M orexin A. The effect of orexin A on the distribution of receptors between the cell surface and cytoplasm was assessed by an inverted Nikon TE2000-E microscope. Sequential images were acquired at 10-min intervals for 30-min time period.

Detection of Internalization (Biotinylation)—Cells were grown and induced overnight with 100 ng·ml^{-1} doxycycline in 6-well plates treated with 0.1 mg·ml^{-1} poly-D-lysine. Ligand treatments were carried out as required. The plates were put on ice, the medium was removed and the cells washed with 2 ml/well ice cold borate buffer (10 mM boric acid, 154 mM NaCl, 7.2 mM KCl 1.8 mM $CaCl_2$, pH 9.0). 1 ml/well 0.8 mM Sulfo-NHS-SS-Biotin (Pierce, Thermo Scientific), in borate buffer, was added, and the plates incubated on ice, in the dark, for 30 min. The biotin solution was removed, the cells washed with 2 ml/well stop solution (192 mM glycine, 25 mM Tris-HCl, pH 8.3), and incubated with a further 2 ml/well stop solution for 5 min on ice. The stop solution was removed, and the cells lysed by the addition of 500–1000 μl 1× RIPA. The plates were scraped and the lysates transferred to Eppendorf tubes, which were then end over end mixed at 4 °C for 15 min, before being centrifuged at 18,000 × *g* for 10 min at 4 °C. The protein concentrations of the supernatants were determined and equalized (lysate samples were taken for later analysis). 100 μl/tube streptavidin-agarose resin (Pierce, Thermo Scientific) was added, and tubes incubated on a rotating wheel at 4 °C overnight before being centrifuged at 2000 × *g* for 2 min at 4 °C. The supernatant was removed, and the resin washed with 3 × 500 μl RIPA buffer. 100 μl of SDS-PAGE sample buffer containing 5% 2-mercaptoethanol was added, and tubes incubated at 37 °C for 1 h. The cell lysates and biotinylated samples were then subjected to SDS-PAGE analysis and Western blotting as described above.

Combined FlAsH Labeling and Calcium Loading of X-rhod-1 AM—Cells were grown on poly-D-lysine-treated glass coverslips and induced with 100 ng·ml^{-1} doxycycline for 48 h. The coverslips (with cells attached) were then transferred to 6-well plates containing 2 ml per well of (phenol red free) Hank's balanced salt solution, supplemented with 10 mM glucose (control HBSS). Each well was washed three times (10 min per wash) with control HBSS. After washing, 1.8 ml of control HBSS was added to each well. FlAsH labeling solution (sufficient for 1 × 6 well plate), was prepared by adding 6 μl of 2 mM lumiogreen stock solution (Invitrogen), to 6 μl of 25 mM ethanedithiol (EDT) solution in DMSO (2.1 μl of EDT in 1 ml DMSO). This solution was incubated at room temperature for 20 min. 1.2 ml of control HBSS solution was added and vortex mixed. The EDT/FIAsH/HBSS solution was then allowed to stand for a further 20 min in the dark. 200 μl aliquots of the EDT/FIAsH/HBSS solution were then added to each of the wells containing 1.8 ml of control HBSS. The plate was then gently swirled to ensure uniform distribution of the labeling solution and incubated at 37 °C for 1 h in the dark. During this incubation period, EDT/HBSS washing solution was prepared by mixing 42 μl of EDT with 1 ml of DMSO, (500 mM EDT in DMSO). 25 μl of this was added to 50 ml of control HBSS and mixed to form a control HBSS solution containing 250 μM EDT. After 1 h, the cells were removed from the incubator and the FlAsH labeling solution removed and replaced with 3 ml of EDT/HBSS wash solution. Cells were incubated for 15 min in the dark to reduce nonspecifically bound FlAsH. The wash was repeated twice. Cells were then rinsed three times, (5 min/wash), with control HBSS to ensure complete removal of EDT from labeled cells. These labeled cells were then stored at room temperature in the dark or were transferred into fresh growth medium and loaded with the membrane-permeant Ca^{2+}-sensitive dye X-rhod-1 AM, (3 μM), for 30 min at 37 °C.

Combined FlAsH FRET and Ca^{2+}-imaging Experiments—Washed FlAsH-labeled cells were placed into a microscope chamber containing physiological HEPES-buffered saline solution (130 mM NaCl, 5 mM KCl, 1 mM $CaCl_2$, 1 mM $MgCl_2$, 20 mM HEPES, and 10 mM D-glucose, pH 7.4). Cells were then imaged using an inverted Nikon TE2000-E microscope (Nikon Instruments) equipped with a ×40 (numerical aperture = 1.3) oil immersion Fluor lens. Excitation light was generated from a computer-controlled Optoscan monochromator (Cairn Research, Faversham, UK), which was coupled to an ultra-highpoint intensity Optosource lamp, (Cairn Research), fitted with a 103 watt mercury arc lamp (Osram 103W/2). Monochromator was set to 427 nm/bandwidth, (BW) 5 nm or 504 nm/BW 5 nm, to visualize surface located CFP-tagged receptors labeled with FlAsH. Excitation light, (427 nm or 504 nm), was reflected through the Fluor objective lens using a cyan/yellow fluorescent protein dual band dichroic filter (Semrock; Rochester, NY, catalogue no. FF440/520-Di01), mounted in the microscope. FRET and donor emission images were recorded exactly at the same time interval using a Quadview 2, (QV2), image splitting device, (Photometrics, UK), coupled to a CoolSnap-HQ2 camera connected to the microscope's bottom port for maximal detection of emitted fluorescence. FRET, donor and calcium signals were detected simultaneously using the following Chroma (Chroma, Brattleboro, VT), ET series dichroic and emitters mounted in the QV2 cube: ET t505LPXR dichroic, ET535/30 nm, ET 470/30 nn, ET 632/60 nm. Using the streaming capability of the multiple dimensional wavelength acquisition module of MetaMorph, ligand-induced changes in intramolecular FRET and simultaneous elevation of intracellular free Ca^{2+} were recorded at 40 ms intervals during excitation with 427 nm light directly to the computer's hard drive. The Cool Snap-HQ2 camera was operated in 14-bit mode and exposure time, binning (8 × 8), and camera gain, were kept constant for all streaming experiments. Computer control of all electronic hardware and camera streaming acquisition was achieved using Metamorph software (version 7.7.5 Molecular Devices, Sunnydale, CA). TTL controlled solenoid valves connected to a peristaltic pump operated at a flow rate of 5 ml/min were used to rapidly add or remove test ligands into the imaging chamber.

Ratiometric Quantification of Changes in Intramolecular FlAsH FRET and Elevation of Cytosolic-free Ca^{2+}—Using Metamorph's split view module, saved images were split to form individual FRET, donor, and calcium stream time-lapse stacks. Each stack was corrected for background fluorescence and exported into Metamorph's align module to ensure that there was no x or y pixel shift misalignment between the donor, FRET and calcium channel stream stacks prior to the calculation of the intramolecular FRET ratio values or Delta F/F0 calcium ratio values. Changes in intramolecular FRET or combined intramolecular FRET intracellular calcium were measured by manually drawing regions of interest, (ROI), around the profile of individual cells and averaging the signals within the delimited ROI for each time-lapse image collected at 470, 535 or 630 nm emission. Ratiometric FRET values were

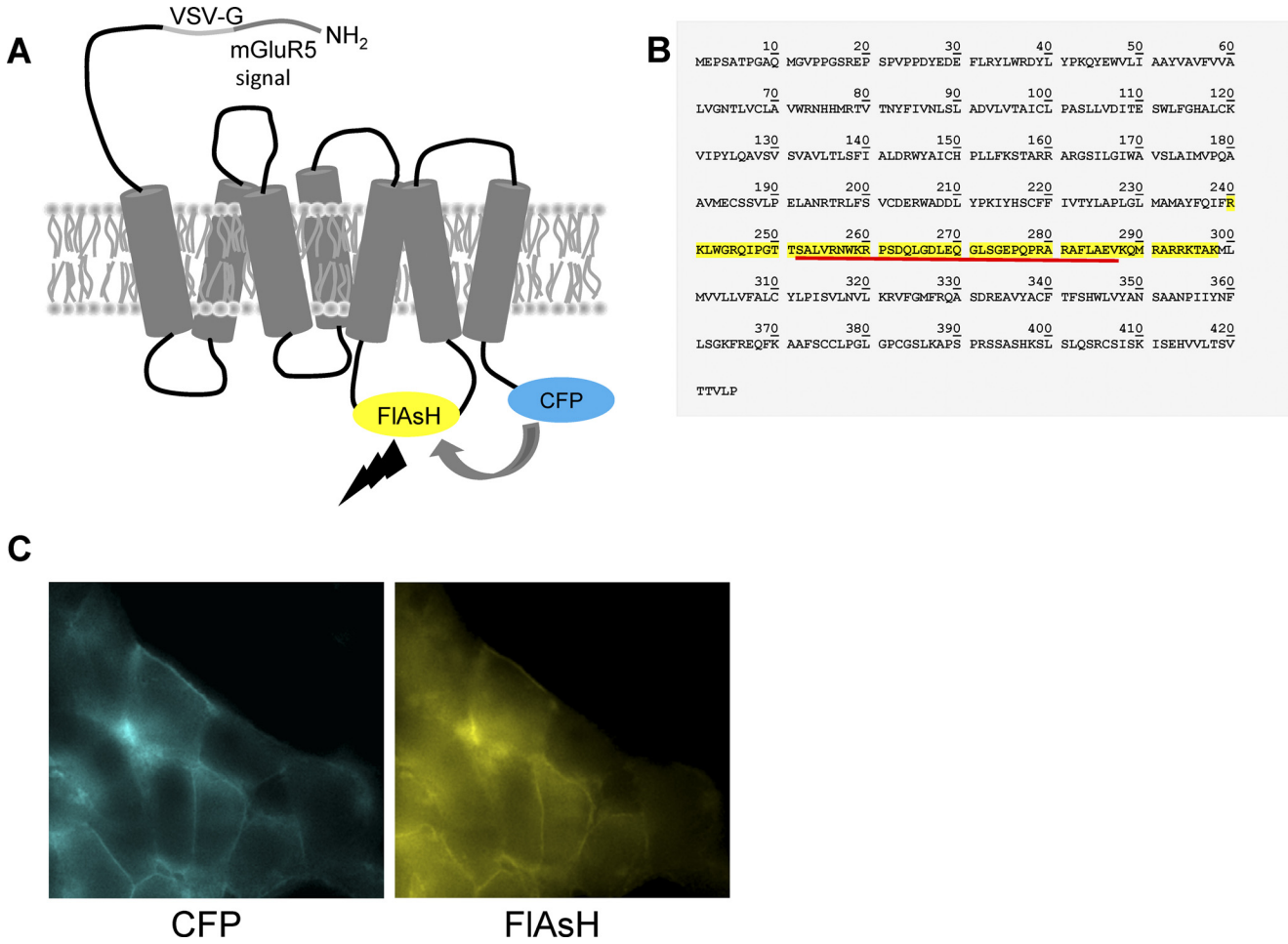

FIGURE 1. **Organization and expression of an OX_1 FRET sensor.** *A*, human OX_1 receptor was modified at the N terminus by addition of a leader sequence from the metabotropic glutamate 5 receptor (*mGluR5*) followed by the VSV-G peptide epitope sequence while cyan fluorescent protein (*CFP*) was added in-frame at the C terminus. The FlAsH motif sequence FLNCCPGCCMEP was introduced into the third intracellular loop (predicted region highlighted in *yellow* in *B*) that links transmembrane domains V and VI. Energy transfer from CFP to FlAsH and subsequent output is illustrated. *B*, primary amino acid sequence of the human OX_1 receptor. In the sensor used for the studies reported, the FlAsH motif replaced the sequence underlined in red. This procedure shortened the predicted length of the third intracellular loop from 59 to 36 amino acids. *C*, following cloning into the inducible Flp-In™ T-REx™ locus of Flp-In™ T-REx™ 293 cells and induction of expression by addition of doxycycline, imaging of CFP (*left hand panel*) or the labeled FlAsH motif (*right hand panel*) demonstrated effective delivery of this sensor to the cell surface.

then calculated as the average 535 nm emission intensity divided by the average 470 nm emission intensity. Delta F/F0 calcium ratio values were measured by quantifying the difference between the calcium fluorescence signal intensity and the baseline calcium fluorescence measured prior to the onset of the calcium signal. Quantified ratio values were exported into Prism 5.02 (GraphPadSoftware Inc.) and using Graphpad's transforming module, FRET ratiometric were set to a value of 1.0 at the onset of each experiment and plotted over time. Control experiments were set up to ensure that the X-rhod-1 dye emitted fluorescence did not bleed through into the donor or FRET channel of the QV2 image splitter. No eCFP or FlAsH emitted fluorescence was detected in the 630 nm emission channel of the QV2.

RESULTS

Generation and Expression of Potential Intramolecular OX_1 Receptor FRET Sensors—Intramolecular FRET sensors can provide a powerful means to explore ligand binding and activation kinetics of GPCRs (27). However, the very limited number of sensors described to date (17, 20–23, 28) suggests that the production of effective constructs is challenging. To generate such a sensor for the orexin OX_1 receptor we added CFP in-frame with the C-terminal tail of the full-length human OX_1 receptor or to C-terminally truncated variants (supplemental Fig. S1). These also contained the VSV-G peptide epitope within the extracellular N-terminal domain (Fig. 1*A*). Based on a published sensor for the muscarinic M_3 acetylcholine receptor (23, 28), like OX_1 also a predominantly $G\alpha_{q/11}$-coupled receptor, we then inserted the 12 amino acid sequence, FLNCCPGCCMEP, containing the minimal fluorescein arsenical hairpin binder via tetra-cysteine (FlAsH) labeling sequence, CCPGCC, into the third intracellular loop of these OX_1 receptor variants (Fig. 1*A* and supplemental Fig. S1). During this process either an equivalent 12 amino acid segment (^{263}DQLGDLEQGLSG^{274}) of the receptor was replaced to maintain the overall predicted size of this loop at 59 amino acids, or the overall length of this loop was shortened to 36 amino acids by replacing the sequence ^{252}SALVRNWKRPSDQLGDLEQGLSGEPQPRARAFLAE^{286} from the central segment of this loop (Fig. 1*B* and supplemental Fig. S1). We also generated a form of the potential sensor in

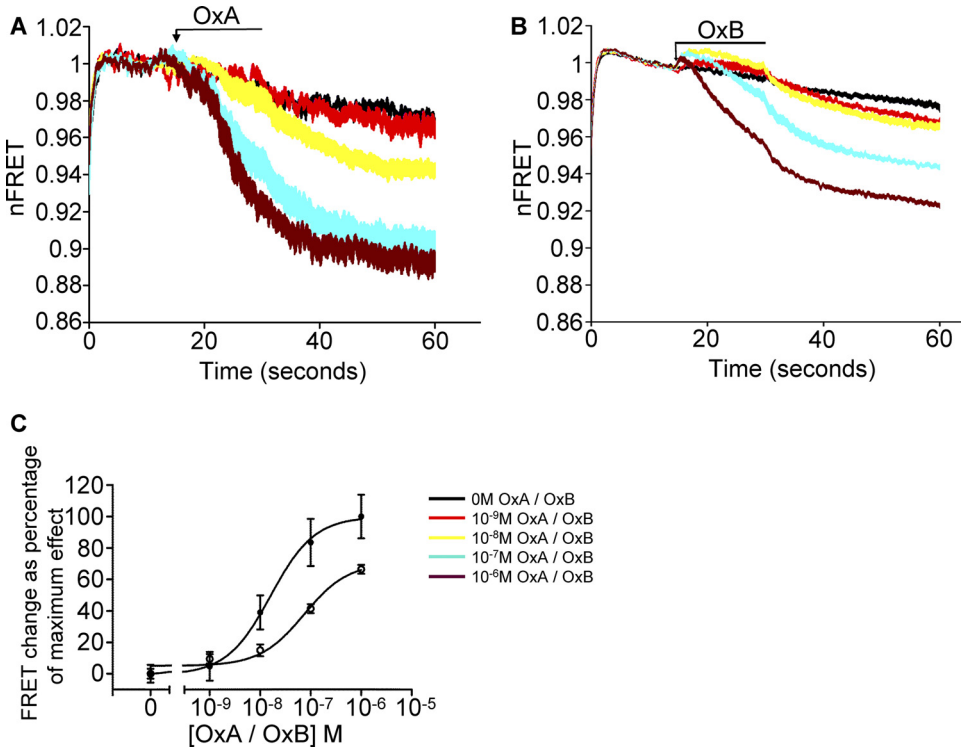

FIGURE 2. **Response of an OX_1 intramolecular FRET sensor to orexin peptides is both time- and concentration-dependent.** Flp-In™ T-REx™ 293 cells induced to express mGluR5-VSV-G-OX_1-FlAsH-CFP were employed in FRET imaging studies. *A* and *B*, various concentrations of orexin A (*OxA*)(*A*) or orexin B (*OxB*) (*B*) were added at the indicated point and FRET signal monitored over the ensuing 45 s period. The orexin peptides were removed after application for 15 s (*bar*). *C*, change in normalized FRET signal from addition of the peptides to the 60 s time point was measured and plotted with the effect of 10^{-6} M orexin A defined as 100% and vehicle as 0%. Data represent means ± S.E., $n = 5$.

which an N-terminal leader sequence from the metabotropic glutamate receptor 5 was added to the extreme N terminus of the construct in which the 3rd intracellular loop was reduced to 36 amino acids to generate mGluR5-VSV-G-OX_1-FlAsH-CFP (Fig. 1*A* and supplemental Fig. S1). Transient transfection into HEK293 cells resulted, however, in limited cell surface delivery of any of these constructs, including mGluR5-VSV-G-OX_1-FlAsH-CFP (supplemental Fig. S1), although such experiments did allow imaging of CFP and successful labeling of the FlAsH sequence of the constructs to generate a potential FRET acceptor (supplemental Fig. S1). Using the mGluR5-VSV-G-OX_1-FlAsH-CFP construct we then generated stable cell lines following transfection of Flp-In™ T-REx™ 293 cells. These cells allow inducible and regulated expression of constructs cloned into the Flp-In™ T-REx™ locus (26). In such cells induction of expression in the presence of doxycycline resulted in effective cell surface delivery of this construct (Fig. 1*C*). Similar cell lines were generated with the other constructs described earlier (not shown).

Preliminary FRET imaging experiments using such cells showed larger changes in FRET signal upon addition of the peptide agonist orexin A for the sensors with the shortened 3rd intracellular loop and cells able to express mGluR5-VSV-G-OX_1-FlAsH-CFP were selected, therefore, for detailed studies. Normalized basal FRET signal in cells induced to express mGluR5-VSV-G-OX_1-FlAsH-CFP was reduced upon addition of orexin A in a time- and concentration-dependent manner (Fig. 2*A*). This was also the case when employing the second endogenously produced orexin peptide, orexin B (Fig. 2*B*). Half-maximal effects of orexin A were produced with $1.6 \pm 0.18 \times 10^{-8}$ M of the peptide (Fig. 2*C*), while orexin B was some 5 fold less potent ($EC_{50} = 7.4 \pm 2.5 \times 10^{-8}$ M) (means ± S.E., $n = 5$). As anticipated from mass-action the observed kinetic of sensor response was slower at lower concentrations of orexin A but with a near maximally effective concentration of orexin A (10^{-6} M) the response was fit by a mono-exponential with $t_{0.5} = 6.8 \pm 0.6$ s (mean ± S.E., $n = 5$). By contrast, addition of the OX_1 antagonist SB408124 (10^{-6} M) did not produce a time-dependent alteration of sensor response beyond the effect of vehicle but, as anticipated, did block the effect of orexin A when the two ligands were co-added (Fig. 3). Removal of orexin A and potential wash out of the ligand did not, however, result in a rapid reversal of the FRET changes (Fig. 3). This is consistent with sustained residency of the agonist on the receptor and, indeed, orexin A has been shown previously to be able to co-internalize from the surface of cells still bound to the OX_1 receptor (29).

To compare the kinetic of receptor activation with that of signal generation we loaded cells induced to express mGluR5-VSV-G-OX_1-FlAsH-CFP with the [Ca^{2+}] sensor dye X-rhod-1 AM (30). This allowed concurrent imaging of the intramolecular re-arrangement of the OX_1-sensor in response to binding of orexin A, by measuring emission from each of CFP and FlAsH, and the elevation of Ca^{2+} (Fig. 4*A*). Although small compared with the maximal alteration of the FRET signal over time, onset of sensor FRET signal alteration could be detected within 1 s of addition of orexin A (10^{-7} M) while initial detection of changes in Ca^{2+} was significantly slower ($p < 0.001$) requiring some 4 s

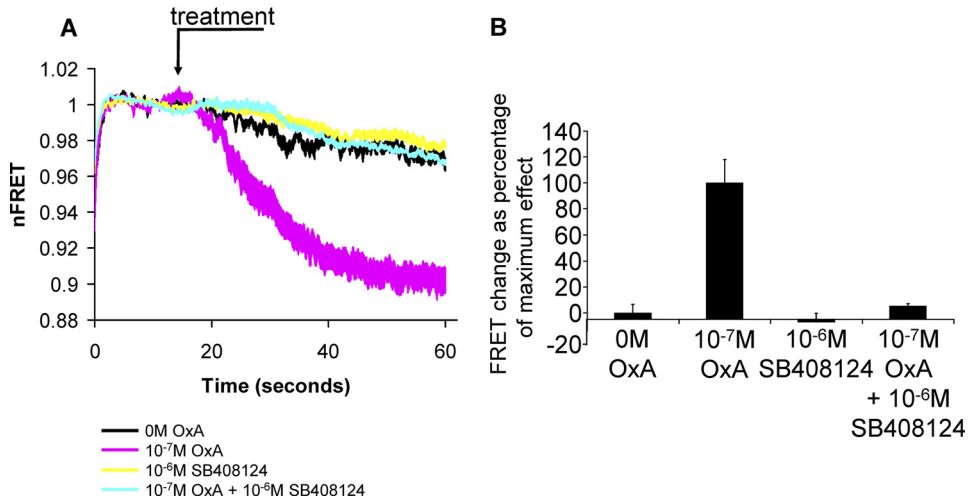

FIGURE 3. **Effects of orexin A at the OX_1 intramolecular FRET sensor are prevented by co-addition of an OX_1 receptor antagonist.** Studies were conducted as in Fig. 2. The OX_1 receptor antagonist SB408124 (13) did not modulate the FRET signal of mGluR5-VSV-G-OX_1-FlAsH-CFP but co-addition with orexin A blocked the effect of the agonist (*A*). Studies are quantified in *B*. Data represent means ± S.E., $n = 5$.

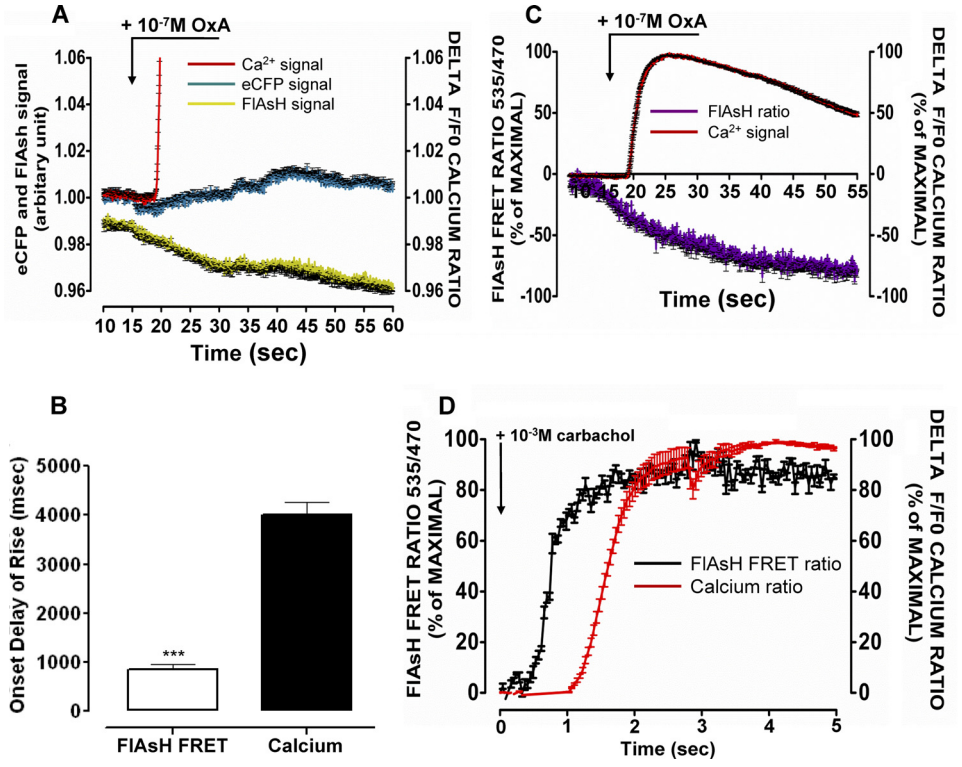

FIGURE 4. **Comparisons of the responsiveness of the OX_1 and muscarinic M_3 FRET sensors.** Cells induced to express mGluR5-VSV-G-OX_1-FlAsH-CFP were labeled with lumiogreen and loaded with X-rhod-1 AM. Following addition of orexin A (10^{-7} M) fluorescence corresponding to CFP (*cyan*), the FlAsH sensor (*yellow*) and alterations in $[Ca^{2+}]$ (*red*) were monitored over time (*A*). In *B*, the period of time before statistically significant changes in CFP-FlAsH FRET or $[Ca^{2+}]_i$ were recorded are displayed. The $[Ca^{2+}]_i$ response was significantly slower than the FRET response (***, $p < 0.001$). *C*, an extended time course of the $[Ca^{2+}]_i$ response (*red*) is compared with the change in FRET (*purple*). *D*, similar studies were performed using cells induced to express a muscarinic M_3 receptor FRET sensor (23) to which the agonist carbachol (10^{-3} M) was added at time = 0. *Black*, FRET signal, *red*, calcium response.

(Fig. 4*B*) and reached maximal levels by 10 s before decaying toward basal levels while the alteration in FRET signal was maintained (Fig. 4*C*). These studies cannot define whether these time differences indicate that the OX_1 receptor continues to re-arrange following agonist binding and G protein engagement and activation or whether a substantial receptor reserve exists such that activation of a small proportion of the expressed receptors is sufficient to trigger the Ca^{2+} response. However, studies performed with different orexin A concentrations indicated that the sensor response was at least as sensitive to the ligand as the Ca^{2+} response (supplemental Fig. S2), suggesting that there is not a large receptor reserve. The kinetic responses of the OX_1 receptor were in marked contrast to equivalent studies performed using a similar muscarinic M_3 acetylcholine receptor sensor (23). Here, the $t_{0.5}$ for sensor response following addition of a maximally effective concentration (10^{-3} M) of the synthetic agonist carbachol was less than 0.2 s (Fig. 4*D*), and the FRET alteration of the sensor was essen-

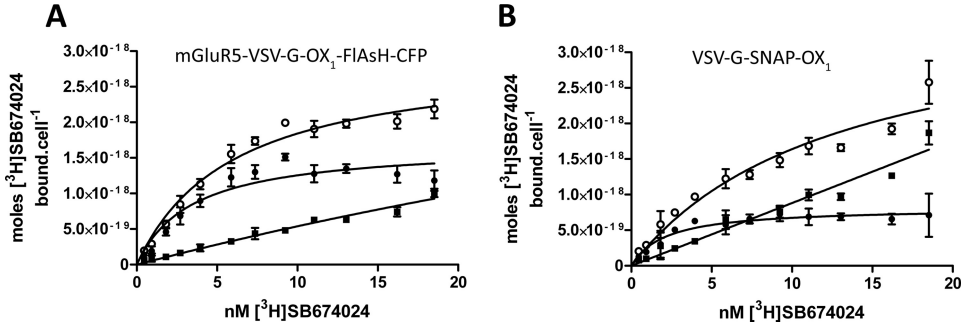

FIGURE 5. **Modifications to generate the OX_1 intramolecular FRET sensor do not alter the ligand binding characteristics of the receptor.** Saturation [^{3}H]SB674042 binding studies were performed on intact Flp-In^{TM} T-REx^{TM} 293 cells induced to express mGluR5-VSV-G-OX_1-FlAsH-CFP (*A*) and compared with equivalent studies performed on cells induced to express a second OX_1 receptor construct VSV-G SNAP-OX_1 (*B*), previously characterized in (23–24). Total binding (*open circles*), nonspecific binding (*filled squares*), and specific binding (*filled circles*) were assessed. Experiments shown are representative of $n = 3$.

tially complete (< 1 s) before any elevation of Ca^{2+} could be detected (Fig. 4*D*). Furthermore, as reported previously (23), and currently mainly limited among such intramolecular FRET sensors to the muscarinic receptor subtypes, M_1, M_3, and M_5, that couple selectively to the G_q/G_{11} pathway (28), addition of carbachol to cells expressing the muscarinic M_3 acetylcholine receptor sensor resulted in a rapid increase, rather than decrease, in the normalized FRET signal.

Functional Characterization of the Intramolecular OX_1 Receptor FRET Sensor—Cells induced to express mGluR5-VSV-G-OX_1-FlAsH-CFP were used in intact cell ligand binding studies using the OX_1 antagonist [^{3}H]SB674042 (13, 24–25, 31). These studies indicated that the sensor construct bound this ligand with nanomolar affinity (K_d = 2.56 ± 0.34 nM, mean ± S.E., $n = 5$) (Fig. 5*A*) unchanged from that observed for a previously described N-terminally SNAP-tagged form of the OX_1 receptor (VSV-G-SNAP-OX_1) (25, 31) (K_d = 2.21 ± 0.39 nM, mean ± S.E., $n = 5$) (Fig. 5*B*) that does not have any alterations within the intracellular segments of the receptor. This is also similar to values reported in earlier intact cell ligand binding studies performed on the unmodified OX_1 receptor (13). Equivalent binding studies performed on membrane preparations derived from these cells also demonstrated similar binding affinity of [^{3}H]SB674042 to the two forms of the OX_1 receptor (mGluR5-VSV-G-OX_1-FlAsH-CFP K_d = 0.97 ± 0.16 nM and VSV-G-SNAP-OX_1 K_d = 1.09 ± 0.12 nM, means ± S.E., $n = 3$) (supplemental Fig. S3). Furthermore, other antagonists with OX_1 affinity, including SB334867 (pK_i = 6.87 ± 0.15) and SB408124 (pK_i = 7.36 ± 0.04), were able to compete with [^{3}H]SB674042 for binding to mGluR5-VSV-G-OX_1-FlAsH-CFP in both membrane preparations (supplemental Fig. S3) and intact cells (not shown), whereas the selective OX_2 receptor antagonist TCS-OX2–29 (32–33) was in the region of 100 fold less potent (pK_i = 4.92 ± 0.13) than either of the OX_1 selective antagonists (supplemental Fig. S3).

The functionality of the mGluR5-VSV-G-OX_1-FlAsH-CFP construct was assessed initially in cell population [Ca^{2+}] studies. Here orexin A produced elevation of $[Ca^{2+}]_i$ with pEC_{50} = 6.36 ± 0.06 (mean ± S.E., $n = 3$) in cells induced to express the mGluR5-VSV-G-OX_1-FlAsH-CFP sensor while no response to orexin A was observed in cells harboring the construct but in which expression had not been induced by prior treatment with doxycycline (Fig. 6*A*). Orexin A was also able to promote phosphorylation of the ERK1/2 MAP kinases in a time- (supplemental Fig. S4) and concentration- (pEC_{50} = 7.53 ± 0.12, mean ± S.E., $n = 3$) dependent manner (Fig. 6*B*). Orexin B, the second endogenously produced orexin peptide, also promoted phosphorylation of the ERK1/2 MAP kinases via the sensor construct but with some 10-fold lower potency (pEC_{50} = 6.50 ± 0.33) (Fig. 6*B*) while, as anticipated from previous studies (34), an N-terminally truncated form of orexin A (orexin A 16–33), although displaying activity, was significantly less potent (pEC_{50} = 5.72 ± 0.09) (Fig. 6*B*). The OX_1 selective antagonist SB408124 at 1×10^{-6} M inhibited the effect of orexin A (supplemental Fig. S4) whereas, at this concentration, the OX_2 selective antagonist TCS-OX2–29 was without significant effect (supplemental Fig. S4). Although requiring high concentrations to induce a reduction in intramolecular FRET signal, orexin A (16–33) also functioned as an agonist at the mGluR5-VSV-G-OX_1-FlAsH-CFP sensor (Fig. 6*C*).

As with other forms of the OX_1 receptor (24–25, 29) sustained treatment of the cells with orexin A resulted in marked time-and concentration-dependent internalization of mGluR5-VSV-G-OX_1-FlAsH-CFP. Confocal imaging of the CFP tag in cells induced to express mGluR5-VSV-G-OX_1-FlAsH-CFP demonstrated movement of the receptor from the cell surface to punctate intracellular vesicles (Fig. 7*A*). To quantify this process and provide a measure of the potency of orexin A we employed cell surface biotinylation studies. Cells induced to express mGluR5-VSV-G-OX_1-FlAsH-CFP were either treated with 10^{-6} M orexin A for up to 90 min or with varying concentrations of orexin A for 40 min, and then cell surface proteins were labeled with biotin. Following capture with streptavidin and separation by SDS-PAGE samples were immunoblotted with anti-VSV-G to detect the FRET sensor. In the absence of orexin A an apparently single polypeptide with mobility corresponding to 80 kDa was identified (Fig. 7*B*). This clearly corresponded to mGluR5-VSV-G-OX_1-FlAsH-CFP because no such polypeptide was identified when equivalent experiments were performed on cells in which expression of the construct had not been induced (Fig. 7*B*). Following treatment with orexin A the level of biotinylated polypeptide detected with anti-VSV-G was reduced, consistent with removal of a proportion of the receptor from the cell surface. The estimated pEC_{50} for orexin A was 7.98 ± 0.36 (Fig. 7*B*) while the half-time for 10^{-6} M orexin A to produce internalization was 17.4 ± 3.2

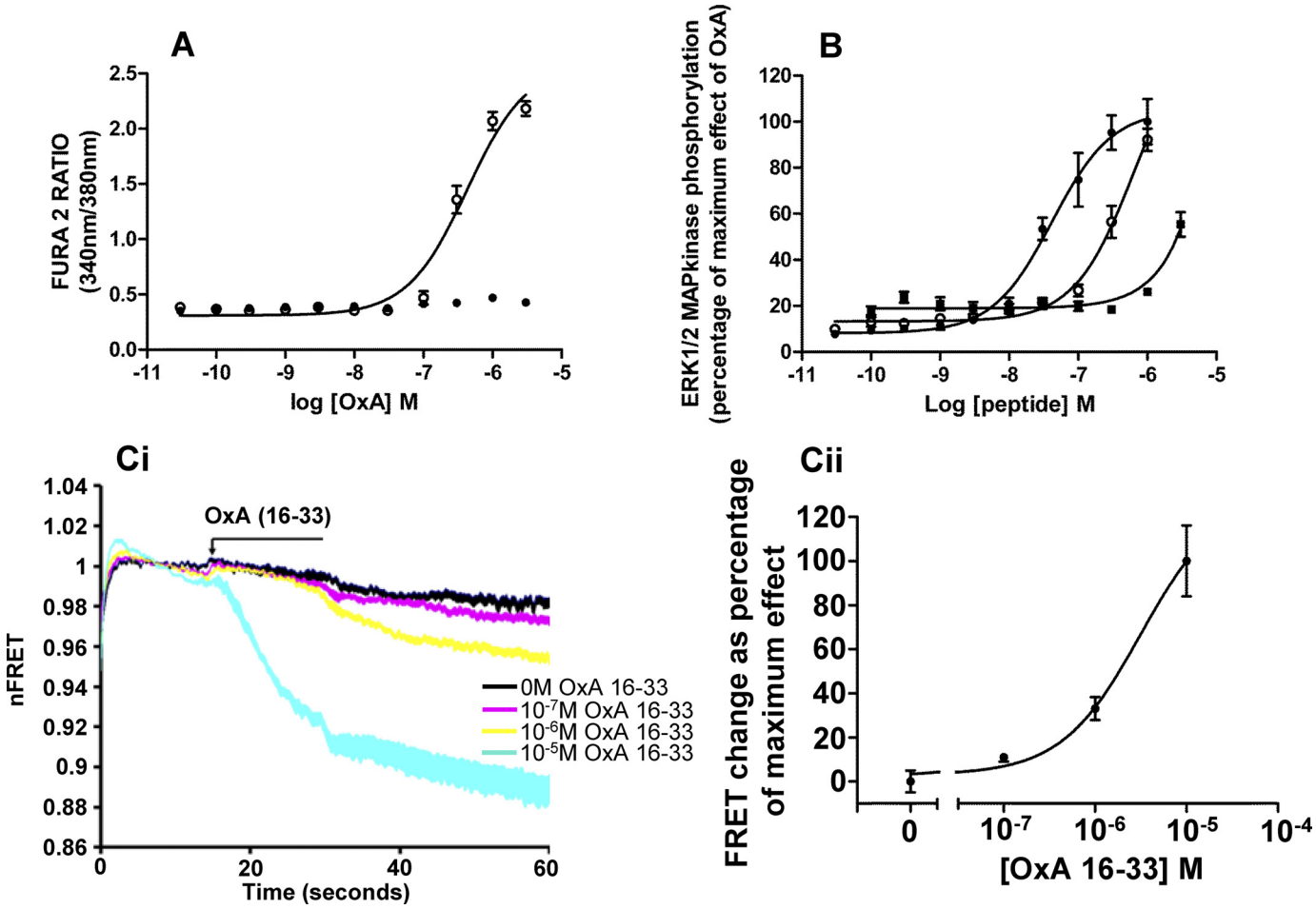

FIGURE 6. **The OX_1 intramolecular FRET sensor is functional.** *A*, Flp-In™ T-REx™ 293 cells harboring mGluR5-VSV-G-OX_1-FlAsH-CFP were either untreated (*filled symbols*) or induced to express the OX_1 sensor (*open symbols*) by treatment with doxycycline (100 ng·ml^{-1}, 24 h). Cells were then loaded with the ratiometric Ca^{2+} indicator dye Fura-2 AM, challenged with varying concentrations of orexin A and elevation of $[Ca^{2+}]_i$ assessed (combined results of $n = 3$). *B*, cells induced to express mGluR5-VSV-G-OX_1-FlAsH-CFP were used in ERK1/2 MAP kinase phosphorylation assays with ligand-induced phosphorylation measured using the SureFire assay kit. Orexin A, *filled circles*; orexin B, *open circles*; orexin A 16–33, *filled squares* (combined results of $n = 3$). *C*, although of low potency, orexin A 16–33 was also able to activate the mGluR5-VSV-G-OX_1-FlAsH-CFP sensor. (*Ci*) the kinetic of response and (*Cii*) the relative maximal effect of varying concentrations of orexin A 16–33 are shown.

min (means ± S.E., $n = 3$) (Fig. 7*B*). Internalization of the OX_1 receptor in HEK293 cells is clathrin-dependent and blocked by elevated osmolality (29). Thus, although neither the biotinylation nor the microscopy studies indicated internalization of mGluR5-VSV-G-OX_1-FlAsH-CFP within the time scale of the sensor response, we performed further studies in the presence of 0.4 M sucrose to block any such effect. Neither the time-course nor the extent of FRET response of the sensor to 10^{-7} M orexin A was affected (supplemental Fig. S5).

Mutation of Asp-203 in OX_1 Retains Antagonist Affinity but Greatly Reduces Potency of Orexin A—Previous mutagenesis studies have indicated that alteration of Asp-203 to Ala in the OX_1 receptor greatly reduces the potency of orexin A while having limited effects on the binding affinity of antagonists including [^{3}H]SB674042 (14). After introduction of this alteration into the mGluR5-VSV-G-OX_1-FlAsH-CFP sensor a further Flp-In™ T-REx™ 293 cell line able to express this construct only in the presence of doxycycline was produced. Consistent with the results of (14) membranes from these cells bound [^{3}H]SB674042 with affinity (K_d = 0.48 ± 0.12 nM, mean ± S.E., $n = 3$) (Fig. 8*A*) similar to the wild type OX_1 sensor, whereas even at the highest concentration of orexin A that could be used (1×10^{-5} M) only small effects on phosphorylation of the ERK1/2 MAP kinases were detected (Fig. 8*B*). Consistent with the loss of agonist potency, this form of the FRET sensor failed to respond to the addition of orexin A (1×10^{-6} M) (Fig. 8*C*).

An Intramolecular OX_2 Receptor FRET Sensor—While the OX_1 receptor is an interesting target for the design of therapeutic small molecule drugs, studies of both narcoleptic dogs and humans have suggested that the OX_2 receptor might be an even more relevant target for treatment of insomnia (1, 7, 9–11). We therefore constructed a series of potential human OX_2 receptor intramolecular FRET sensors using the same principles as for OX_1 except that an HA rather than a VSV-G epitope tag was introduced into the N-terminal domain. As the C-terminal tail of the human OX_2 receptor is predicted to be rather longer (78 amino acids) than OX_1 (65 amino acids) we initially placed CFP at the end of the full-length receptor or truncated this region to 60 amino acids. Similarly we either introduced the FlAsH sequence FLNCCPGCCMEP into the third intracellular loop as replacement for the sequence ^{270}QPVSQPRGPGQP^{281} to

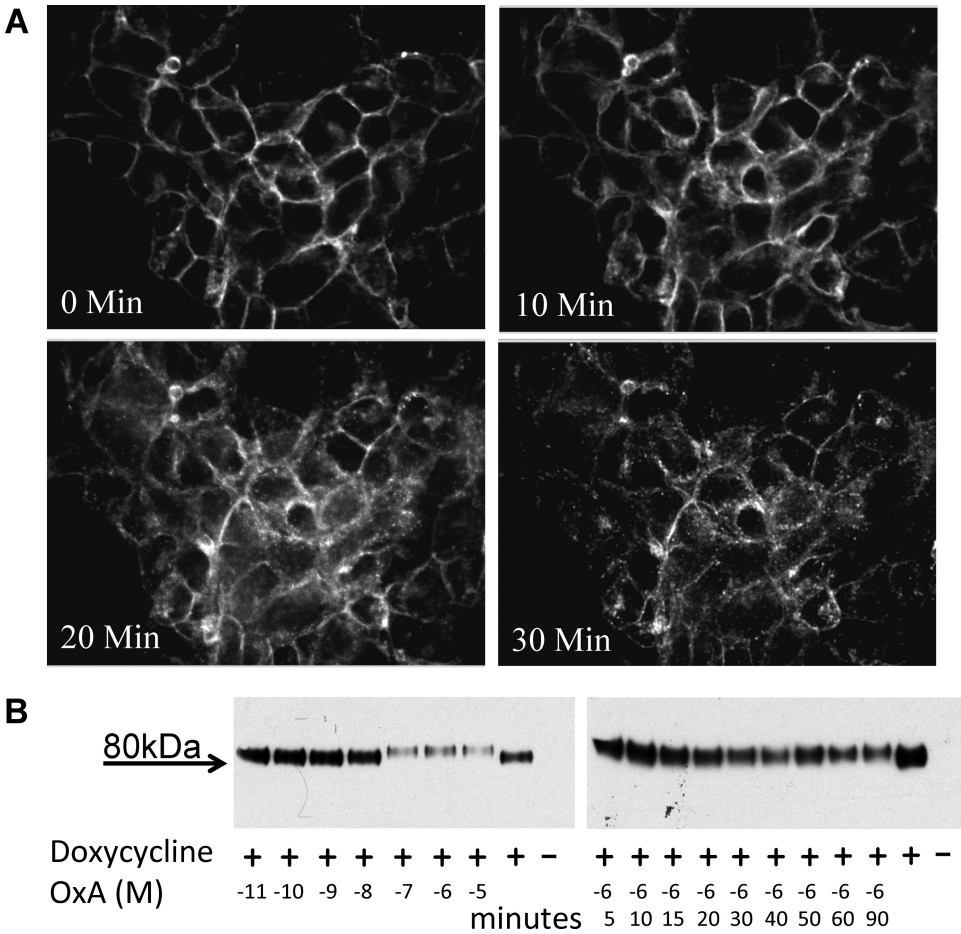

FIGURE 7. **The OX_1 intramolecular FRET sensor becomes internalized in response to orexin A.** *A*, Flp-In™ T-REx™ 293 cells induced to express mGluR5-VSV-G-OX_1-FlAsH-CFP were imaged to detect CFP at various times following addition of orexin A (10^{-7} M). *B*, cell surface biotinylation studies were performed on Flp-In™ T-REx™ 293 cells harboring mGluR5-VSV-G-OX_1-FlAsH-CFP that were either uninduced (− *doxycycline*) or induced to express the sensor (+ *doxycycline*). In the induced cells varying concentrations of orexin A were added for 40 min (*left hand panel*) or 1×10^{-6} M orexin A was added for varying times (*right hand panel*) prior to biotinylation. Cell surface biotinylated proteins were captured, resolved by SDS-PAGE, and mGluR5-VSV-G-OX_1-FlAsH-CFP detected by immunoblotting with anti-VSV-G. Orexin A induced internalization, and therefore reduced the amount of cell surface mGluR5-VSV-G-OX_1-FlAsH-CFP available to be biotinylated, in both a concentration- and time-dependent fashion. Representative examples are shown of $n = 3$ independent experiments.

maintain the loop as 57 amino acids or reduced the overall length to 40 amino acids by substituting the sequence ^{262}VQRKWKPLQPVSQPRGPGQPTKSRMSAVA^{290}. Following preliminary labeling studies with these constructs we used the HA-OX_2-FlAsH-CFP construct with both the reduced C-terminal tail and 3rd intracellular loop to generate Flp-In™ T-REx™ 293 cells able to express this construct in an inducible fashion. Following induction of expression of HA-OX_2-FlAsH-CFP, addition of orexin A (10^{-7} M) also produced a time-dependent decrease in FRET signal (Fig. 9*A*) while in cells induced to express this construct both orexin A and orexin B were able to promote phosphorylation of the ERK1/2 MAP kinases effectively with $pEC_{50} = 7.35 \pm 0.10$ for orexin A and 7.05 ± 0.13 for orexin B (means ± S.E., $n = 5$) (Fig. 9*B*).

DISCUSSION

Upon binding of agonist ligands GPCRs undergo conformational changes that result in enhanced engagement of G protein with subsequent guanine nucleotide exchange on the G protein and eventual regulation of the production of secondary and tertiary messengers (35–36). Studies employing a range of biophysical techniques have indicated that among conformational re-arrangements of the receptor, alterations in the location and extension of transmembrane helix V and, particularly, helix VI (37–39) occur to promote G protein association. In recent times, these conclusions have been validated at atomic level via x-ray crystallography (40) in which in a β_2-adrenoreceptor-$G_s\alpha$ complex conformational changes in the receptor included a 14 Å outward movement at the cytoplasmic end of transmembrane helix VI and an α-helical extension of the cytoplasmic end of helix V. Although of great importance, such structures define single states captured at a specific moment. However, the kinetics and extent of such significant movements should be highly amenable to detection and analysis via resonance energy transfer techniques. Intramolecular FRET sensors of a small number of GPCRs have been produced to assess this (17–23, 41). Based on the anticipated movements of transmembrane helices V and VI in response to agonist binding, all of these constructs have introduced a FRET reporter into the 3rd intracellular loop that links these helices and placed the FRET partner at or within the C-terminal tail. This location is selected, in part, for convenience and because addition of substantial proteins, such as auto-fluorescent proteins derived from GFP, in

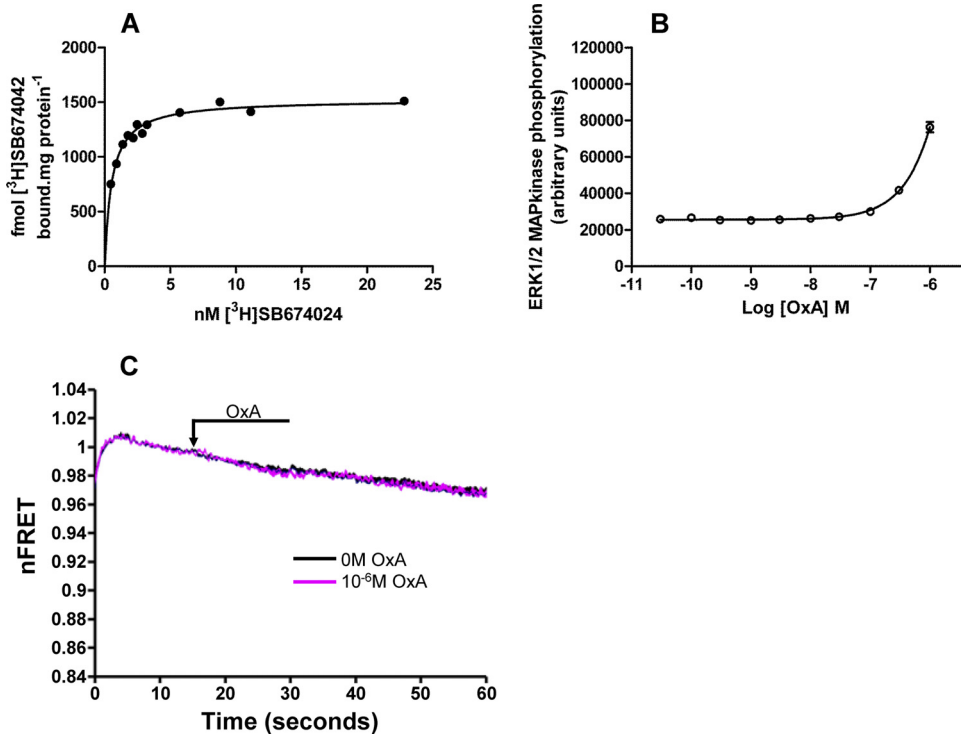

FIGURE 8. **An D203A OX_1 sensor loses potency and responsiveness to orexin A but not affinity for antagonists.** An D203A mutation was introduced into mGluR5-VSV-G-OX_1-FlAsH-CFP. Flp-In™ T-REx™ 293 cells able to express this variant in response to doxycycline were generated. *A*, saturation [^{3}H]SB674042 binding studies were performed on membranes of these cells as in supplemental Fig. S3. Experiments shown are representative of $n = 3$, and specific binding of the ligand is shown. *B*, ability of various concentrations of orexin A to promote ERK1/2 MAP kinase phosphorylation via the D203A OX_1 sensor was quantified using the SureFire assay kit. The pEC_{50} of orexin A at this variant was >6.0. *C*, responsiveness of the sensor to a high concentration of orexin A (1×10^{-6} M) was also assessed.

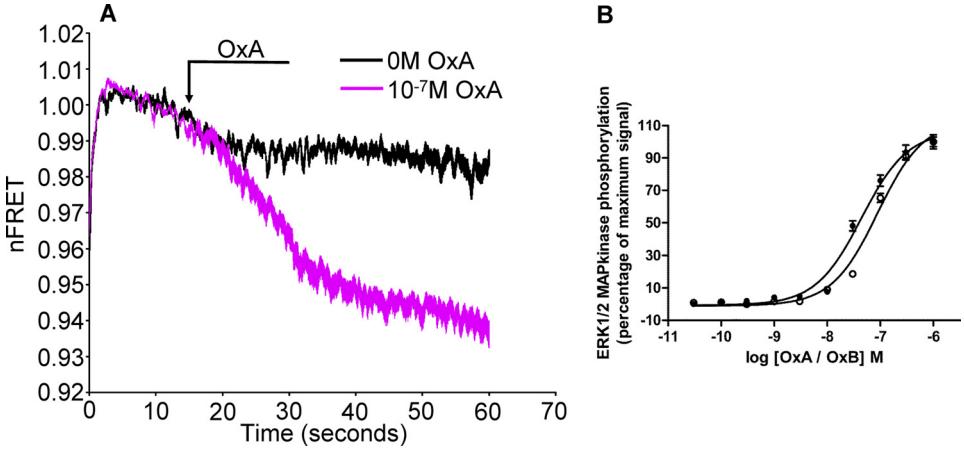

FIGURE 9. **Production and function of an intramolecular FRET sensor for the orexin OX_2 receptor.** A similar approach to that of Fig. 1 and supplemental Fig. S1 was taken to generate potential orexin OX_2 receptor FRET sensors. See "Results" for details. Flp-In™ T-REx™ 293 cells harboring HA-OX_2-FlAsH-CFP were induced to express the construct and (*A*) the ability of orexin A (10^{-7} M) to modulate the basal FRET signal measured over time. *B*, functionality of this construct was assessed in ERK1/2 MAP kinase phosphorylation studies using the SureFire assay kit in response to varying concentration of orexin A (*filled symbols*) or orexin B (*open symbols*) (means ± S.E., $n = 3$).

this region generally has limited effect on the pharmacology and function of receptors. Following expression of such sensors in mammalian cells, in different examples, addition of agonist has resulted in either a time-dependent decrease or increase in basal FRET. At least conceptually, agonist-induced decreases in FRET are consistent with the two FRET partners moving away from each other while an increase in FRET is consistent with the opposite (35). As there are other potential explanations, and nothing is known about how the C-terminal region of GPCRs may move or re-organize in response to agonist occupancy, it is not possible to use these differences to hint at different modes of activation for different receptors but, given the structural information on the β_2-adrenoreceptor it is interesting to note that a FRET sensor of this receptor generated increased FRET signal upon agonist addition (41), distinct from the decrease in intramolecular FRET observed here for both the OX_1 and OX_2 receptor sensors. Despite such issues, intramolecular FRET sensors can provide novel and useful information on the kinetics of response of a GPCR to different ligands and such constructs have also recently been used to detect alterations in

receptor response upon co-addition of orthosteric and allosteric ligands (22). Equally, they have been employed to probe potential alterations in receptor pharmacology upon chemical engineering of a receptor (23) and, on this basis, should also prove useful in studies designed to explore effects on ligand function in point mutants or polymorphic variants of receptors.

Most previously published intramolecular FRET sensors have been based on GPCRs that have small endogenous agonists, such as adrenaline, acetylcholine and adenosine. As noted previously, activation kinetics of such sensors are generally rapid, with estimates of $t_{0.5}$ as low as 50 ms (21) and, herein, using a muscarinic M_3 acetylcholine receptor sensor we record $t_{0.5} = 180$ ms when applying a maximally effective concentration of the acetylcholine mimetic carbachol. As such, the relatively slow response of both OX_1 and OX_2 receptors recorded herein, with $t_{0.5}$ of some 7 s following addition of high concentrations of orexin A, is unlikely to reflect technical limitations with measurement of response. As large peptides the orexins are likely to bind to their receptors via a number of distinct steps and each of these steps may be relatively slow. It was also noted that orexin A was not easily washed out from the sensors. This presumably reflects the high affinity of the peptide for its receptors and, therefore, a likely slow rate of dissociation. Indeed, as with a number of other peptide hormones, orexin A is known to be internalized into cells still bound to the OX_1 receptor (29). It is, therefore, also of interest that a number of receptors have recently been shown to continue to generate G protein-mediated signals following internalization (42–43). Although yet to be explored, FRET sensors such as those described herein could be studied within intracellular locations via application of 2-photon FRET (44) for example.

A key feature of the current studies is that the pharmacology and signaling of the sensors were very similar to the wild type receptors. Although the reported potency of orexin A at the OX_1 receptor varies over a 1000-fold in different studies and in different assays (45) the rank order observed herein of orexin A > orexin B > orexin A 16–33 is recorded routinely. Furthermore, at the OX_2 receptor orexin A and orexin B are generally noted to be essentially equipotent, and results with the OX_2 receptor sensor studied herein are consistent with this. This clearly is of great importance if such sensors are to find a place in providing useful information about activation kinetics and if they might, in time, be expressed transgenically to allow studies to be performed in native cells and tissues both in *ex vivo* and *in vivo* situations. The current studies record the most detailed examination of the functional properties and ligand binding characteristics of any such GPCR FRET sensor. The demonstration that the greatly reduced potency of orexin A at a previously described mutant, D203A, of the OX_1 receptor (14) is retained in the sensor is also of obvious importance in this regard. Although the current sensors are not well suited for *in vivo* studies because of the need to label the FlAsh element and because CFP is not highly quantum efficient, progress in each of these areas is likely to be rapid, with variants of CFP with very high quantum efficiency recently described (46).

There remain many challenges to the widespread development of such intramolecular FRET sensors. Apocryphal stories abound around the need to generate many variants to generate those with sufficient alteration in FRET signal upon ligand addition to be genuinely useful tools, while means to screen rapidly or otherwise predict the behavior of such constructs are not yet available. Despite this, the utility of the sensors reported herein and in previous studies shows their capacity to provide novel insights into the activation processes and kinetics of GPCR function.

REFERENCES

1. Scammell, T. E., and Winrow, C. J. (2011) Orexin receptors: pharmacology and therapeutic opportunities. *Annu. Rev. Pharmacol. Toxicol.* **51,** 243–266
2. Sakurai, T., and Mieda, M. (2011) Connectomics of orexin-producing neurons: interface of systems of emotion, energy homeostasis and arousal. *Trends Pharmacol. Sci.* **32,** 451–462
3. Kodadek, T., and Cai, D. (2010) Chemistry and biology of orexin signaling. *Mol. Biosyst.* **6,** 1366–1375
4. Chiou, L. C., Lee, H. J., Ho, Y. C., Chen, S. P., Liao, Y. Y., Ma, C. H., Fan, P. C., Fuh, J. L., and Wang, S. J. (2010) Orexins/hypocretins: pain regulation and cellular actions. *Curr. Pharm. Des.* **16,** 3089–3100
5. Ritchie, C., Okuro, M., Kanbayashi, T., and Nishino, S. (2010) Hypocretin ligand deficiency in narcolepsy: recent basic and clinical insights. *Curr. Neurol. Neurosci. Rep.* **10,** 180–189
6. Laburthe, M., Voisin, T., and El Firar, A. (2010) Orexins/Hypocretins and orexin receptors in apoptosis: a minireview. *Acta Physiol.* **198,** 393–402
7. Lin, L., Faraco, J., Li, R., Kadotani, H., Rogers, W., Lin, X., Qiu, X., de Jong, P. J., Nishino, S., and Mignot, E. (1999) The sleep disorder canine narcolepsy is caused by a mutation in the hypocretin (orexin) receptor 2 gene. *Cell* **98,** 365–376
8. Tang, J., Chen, J., Ramanjaneya, M., Punn, A., Conner, A. C., and Randeva, H. S. (2008) The signaling profile of recombinant human orexin-2 receptor. *Cell. Signal.* **20,** 1651–1661
9. Neubauer, D. N. (2010) Almorexant, a dual orexin receptor antagonist for the treatment of insomnia. *Curr. Opin. Investig. Drugs* **11,** 101–110
10. Coleman, P. J., Cox, C. D., and Roecker, A. J. (2011) Discovery of dual orexin receptor antagonists (DORAs) for the treatment of insomnia. *Curr. Top. Med. Chem.* **11,** 696–725
11. Winrow, C. J., Gotter, A. L., Cox, C. D., Doran, S. M., Tannenbaum, P. L., Breslin, M. J., Garson, S. L., Fox, S. V., Harrell, C. M., Stevens, J., Reiss, D. R., Cui, D., Coleman, P. J., and Renger, J. J. (2011) Promotion of sleep by suvorexant-a novel dual orexin receptor antagonist. *J. Neurogenet.* **25,** 52–61
12. Bingham, M. J., Cai, J., and Deehan, M. R. (2006) Eating, sleeping, and rewarding: orexin receptors and their antagonists. *Curr. Opin. Drug Discov. Devel.* **9,** 551–559
13. Langmead, C. J., Jerman, J. C., Brough, S. J., Scott, C., Porter, R. A., and Herdon, H. J. (2004) Characterization of the binding of [3H]-SB-674042, a novel nonpeptide antagonist, to the human orexin-1 receptor. *Br. J. Pharmacol.* **141,** 340–346
14. Malherbe, P., Roche, O., Marcuz, A., Kratzeisen, C., Wettstein, J. G., and Bissantz, C. (2010) Mapping the binding pocket of dual antagonist almorexant to human orexin 1 and orexin 2 receptors: comparison with the selective OX1 antagonist SB-674042 and the selective OX2 antagonist *N*-ethyl-2-[(6-methoxy-pyridin-3-yl)-(toluene-2-sulfonyl)-amino]-*N*-pyridin-3-ylmethyl-acetamide (EMPA). *Mol. Pharmacol.* **78,** 81–93
15. Alvarez-Curto, E., Pediani, J. D., and Milligan, G. (2010) Applications of fluorescence and bioluminescence resonance energy transfer to drug discovery at G protein-coupled receptors. *Anal. Bioanal. Chem.* **398,** 167–180
16. Gandía, J., Lluís, C., Ferré, S., Franco, R., and Ciruela, F. (2008) Light resonance energy transfer-based methods in the study of G protein-coupled receptor oligomerization. *Bioessays* **30,** 82–89
17. Hoffmann, C., Gaietta, G., Bünemann, M., Adams, S. R., Oberdorff-Maass, S., Behr, B., Vilardaga, J. P., Tsien, R. Y., Ellisman, M. H., and Lohse, M. J. (2005) A FlAsH-based FRET approach to determine G protein-coupled receptor activation in living cells. *Nat. Methods* **2,** 171–176
18. Zoffmann, S., Bertrand, S., Do, Q. T., Bertrand, D., Rognan, D., Hibert, M.,

and Galzi, J. L. (2007) Topological analysis of the complex formed between neurokinin A and the NK2 tachykinin receptor. *J. Neurochem.* **101,** 506–516
19. Ilien, B., Franchet, C., Bernard, P., Morisset, S., Weill, C. O., Bourguignon, J. J., Hibert, M., and Galzi, J. L. (2003) Fluorescence resonance energy transfer to probe human M1 muscarinic receptor structure and drug binding properties. *J. Neurochem.* **85,** 768–778
20. Chachisvilis, M., Zhang, Y. L., and Frangos, J. A. (2006) G protein-coupled receptors sense fluid shear stress in endothelial cells. *Proc. Natl. Acad. Sci. U.S.A.* **103,** 15463–15468
21. Vilardaga, J. P., Bünemann, M., Krasel, C., Castro, M., and Lohse, M. J. (2003) Measurement of the millisecond activation switch of G protein-coupled receptors in living cells. *Nat. Biotechnol.* **21,** 807–812
22. Maier-Peuschel, M., Frölich, N., Dees, C., Hommers, L. G., Hoffmann, C., Nikolaev, V. O., and Lohse, M. J. (2010) A fluorescence resonance energy transfer-based M2 muscarinic receptor sensor reveals rapid kinetics of allosteric modulation. *J. Biol. Chem.* **285,** 8793–8800
23. Alvarez-Curto, E., Prihandoko, R., Tautermann, C. S., Zwier, J. M., Pediani, J. D., Lohse, M. J., Hoffmann, C., Tobin, A. B., and Milligan, G. (2011) Developing chemical genetic approaches to explore G protein-coupled receptor function: validation of the use of a receptor activated solely by synthetic ligand (RASSL). *Mol. Pharmacol.* **80,** 1033–1046
24. Ward, R. J., Pediani, J. D., and Milligan, G. (2011) Heteromultimerization of cannabinoid CB(1) receptor and orexin OX(1) receptor generates a unique complex in which both protomers are regulated by orexin A. *J. Biol. Chem.* **286,** 37414–37428
25. Ward, R. J., Pediani, J. D., and Milligan, G. (2011) Ligand-induced internalization of the orexin OX(1) and cannabinoid CB(1) receptors assessed via N-terminal SNAP and CLIP-tagging. *Br. J. Pharmacol.* **162,** 1439–1452
26. Ward, R. J., Alvarez-Curto, E., and Milligan G. (2011) Using the Flp-In™ T-Rex™ system to regulate GPCR expression. *Methods Mol. Biol.* **746,** 21–37
27. Lohse, M. J., Nikolaev, V. O., Hein, P., Hoffmann, C., Vilardaga, J. P., and Bünemann, M. (2008) Optical techniques to analyze real-time activation and signaling of G-protein-coupled receptors. *Trends Pharmacol. Sci.* **29,** 159–165
28. Ziegler, N., Bätz, J., Zabel, U., Lohse, M. J., and Hoffmann, C. (2011) FRET-based sensors for the human M1-, M3-, and M5-acetylcholine receptors. *Bioorg. Med. Chem.* **19,** 1048–1054
29. Milasta, S., Evans, N. A., Ormiston, L., Wilson, S., Lefkowitz, R. J., and Milligan, G. (2005) The sustainability of interactions between the orexin-1 receptor and beta-arrestin-2 is defined by a single C-terminal cluster of hydroxy amino acids and modulates the kinetics of ERK MAPK regulation. *Biochem. J.* **387,** 573–584
30. Bolsover, S., Ibrahim, O., O'luanaigh, N., Williams, H., and Cockcroft S. (2001) Use of fluorescent Ca^{2+} dyes with green fluorescent protein and its variants: problems and solutions. *Biochem. J.* **356,** 345–352
31. Xu, T. R., Ward, R. J., Pediani, J. D., and Milligan G. (2011) The orexin OX(1) receptor exists predominantly as a homodimer in the basal state: potential regulation of receptor organization by both agonist and antagonist ligands. *Biochem. J.* **439,** 171–183
32. Roecker, A. J., and Coleman, P. J. (2008) Orexin receptor antagonists: medicinal chemistry and therapeutic potential. *Curr. Top. Med. Chem.* **8,** 977–987
33. Huang, S. C., Dai, Y. W., Lee, Y. H., Chiou, L. C., and Hwang, L. L. (2010) Orexins depolarize rostral ventrolateral medulla neurons and increase arterial pressure and heart rate in rats mainly via orexin 2 receptors. *J. Pharmacol. Exp. Ther.* **334,** 522–529
34. Darker, J. G., Porter, R. A., Eggleston, D. S., Smart, D., Brough, S. J., Sabido-David, C., and Jerman, J. C. (2001) Structure-activity analysis of truncated orexin-A analogues at the orexin-1 receptor. *Bioorg. Med. Chem. Lett.* **11,** 737–740
35. Ambrosio, M., Zürn, A., and Lohse, M. J. (2011) Sensing G-protein-coupled receptor activation. *Neuropharmacol.* **60,** 45–51
36. Lohse, M. J., Hein, P., Hoffmann, C., Nikolaev, V. O., Vilardaga, J. P., and Bünemann M. (2008) Kinetics of G-protein-coupled receptor signals in intact cells. *Br. J. Pharmacol.* **153,** S125–S132
37. Jensen, A. D., Guarnieri, F., Rasmussen, S. G., Asmar, F., Ballesteros, J. A., and Gether U (2001) Agonist-induced conformational changes at the cytoplasmic side of transmembrane segment 6 in the β2 adrenergic receptor mapped by site-selective fluorescent labeling. *J. Biol. Chem.* **276,** 9279–9290
38. Bockenhauer, S., Fürstenberg, A., Yao, X. J., Kobilka, B. K., and Moerner, W. E. (2011) Conformational dynamics of single G protein-coupled receptors in solution. *J. Phys. Chem. B.* **115,** 13328–13338
39. Granier, S., Kim, S., Fung, J. J., Bokoch, M. P., and Parnot C. (2009) FRET-based measurement of GPCR conformational changes. *Methods Mol. Biol.* **552,** 253–268
40. Rasmussen, S. G., Choi, H. J., Fung, J. J., Pardon, E., Casarosa, P., Chae, P. S., Devree, B. T., Rosenbaum, D. M., Thian, F. S., Kobilka, T. S., Schnapp, A., Konetzki, I., Sunahara, R. K., Gellman, S. H., Pautsch, A., Steyaert, J., Weis, W. I., and Kobilka, B. K. (2011) Structure of a nanobody-stabilized active state of the β(2) adrenoceptor. *Nature* **469,** 175–180
41. Nakanishi, J., Takarada, T., Yunoki, S., Kikuchi, Y., and Maeda, M. (2006) FRET-based monitoring of conformational change of the β2 adrenergic receptor in living cells. *Biochem. Biophys. Res. Commun.* **343,** 1191–1196
42. Calebiro, D., Nikolaev, V. O., Persani, L., and Lohse, M. J. (2010) Signaling by internalized G-protein-coupled receptors. *Trends Pharmacol. Sci.* **31,** 221–228
43. Jalink, K., and Moolenaar, W. H. (2010) G protein-coupled receptors: the inside story. *Bioessays* **32,** 13–16
44. Stoneman, M., Singh, D., and Raicu, V. (2011) *In vivo* quantification of G-protein-coupled receptor interactions using spectrally resolved two photon microscopy. *J. Vis. Exp.* **19,** 2247
45. Deleted in proof
46. Adjobo-Hermans, M. J., Goedhart, J., van Weeren, L., Nijmeijer, S., Manders, E. M., Offermanns, S., and Gadella, T. W. Jr. (2011) Real-time visualization of heterotrimeric G protein Gq activation in living cells. *BMC Biol.* **9,** 32